

## $(\text{La}_{1-x}\text{Ba}_x)(\text{Zn}_{1-x}\text{Mn}_x)\text{AsO}$ : A two-dimensional 1111-type diluted magnetic semiconductor in bulk form

Cui Ding,<sup>1</sup> Huiyuan Man,<sup>1</sup> Chuan Qin,<sup>1</sup> Jicai Lu,<sup>1</sup> Yunlei Sun,<sup>1</sup> Quan Wang,<sup>1</sup> Biqiong Yu,<sup>1</sup> Chunmu Feng,<sup>1</sup> T. Goko,<sup>2</sup> C. J. Arguello,<sup>2</sup> L. Liu,<sup>2</sup> B. A. Frandsen,<sup>2</sup> Y. J. Uemura,<sup>2</sup> Hangdong Wang,<sup>3</sup> H. Luetkens,<sup>4</sup> E. Morenzoni,<sup>4</sup> W. Han,<sup>5</sup> C. Q. Jin,<sup>5</sup> T. Munsie,<sup>6</sup> T. J. Williams,<sup>6</sup> R. M. D'Ortenzio,<sup>6</sup> T. Medina,<sup>6</sup> G. M. Luke,<sup>6,7</sup> T. Imai,<sup>6,7</sup> and F. L. Ning<sup>1,\*</sup>

<sup>1</sup>Department of Physics, Zhejiang University, Hangzhou 310027, China

<sup>2</sup>Department of Physics, Columbia University, New York, New York 10027, USA

<sup>3</sup>Department of Physics, Hangzhou Normal University, Hangzhou 310016, China

<sup>4</sup>Laboratory for Muon Spin Spectroscopy, Paul Scherrer Institute, CH-5232 Villigen PSI, Switzerland

<sup>5</sup>Beijing National Laboratory for Condensed Matter Physics and Institute for Physics, Chinese Academy of Sciences, Beijing 100190, China

<sup>6</sup>Department of Physics and Astronomy, McMaster University, Hamilton, Ontario, Canada L8S 4M1

<sup>7</sup>Canadian Institute for Advanced Research, Toronto, Ontario, Canada M5G 1Z8

(Received 22 April 2013; revised manuscript received 13 June 2013; published 2 July 2013)

We report the synthesis and characterization of a bulk diluted magnetic semiconductor  $(\text{La}_{1-x}\text{Ba}_x)(\text{Zn}_{1-x}\text{Mn}_x)\text{AsO}$  ( $0 \leq x \leq 0.2$ ) with a layered crystal structure identical to that of the 1111-type FeAs superconductors. No ferromagnetic order occurs with (Zn,Mn) substitution in the parent compound  $\text{LaZnAsO}$  without charge doping. Together with carrier doping via (La,Ba) substitution, a small amount of Mn substituting for Zn results in ferromagnetic order with  $T_C$  up to  $\sim 40$  K, although the system remains semiconducting. Muon spin relaxation measurements confirm the development of ferromagnetic order in the entire volume, with the relationship between the internal field and  $T_C$  consistent with the trend found in (Ga,Mn)As and the 111-type  $\text{Li}(\text{Zn,Mn})\text{As}$  and the 122-type  $(\text{Ba,K})(\text{Zn,Mn})_2\text{As}_2$  systems.

DOI: [10.1103/PhysRevB.88.041102](https://doi.org/10.1103/PhysRevB.88.041102)

PACS number(s): 75.50.Pp, 71.55.Ht, 76.75.+i

The successful fabrication of III-V ferromagnetic semiconductors (Ga,Mn)As (Ref. 1) in thin-film form via molecular-beam epitaxy (MBE) has triggered extensive research into diluted magnetic semiconductors (DMSs).<sup>2-4</sup> The highest Curie temperature  $T_C$  has been reported as  $\sim 190$  K with Mn doping levels at  $\sim 12\%$  in (Ga,Mn)As.<sup>5</sup> However, the quality of some thin films is strongly dependent on the preparation procedure and heat treatment, and thus not always controllable.<sup>6,7</sup> Nonetheless, if properly prepared, (Ga,Mn)As thin films exhibit spatially homogeneous ferromagnetism throughout the entire sample volume for a wide range of Mn concentrations, as confirmed by muon spin relaxation ( $\mu\text{SR}$ ) measurements.<sup>8</sup> In contrast to the successful use of MBE, the preparation of bulk (Ga,Mn)As has been much more challenging, since the valence mismatch of  $\text{Mn}^{2+}$  atoms and  $\text{Ga}^{3+}$  atoms results in severely limited chemical solubility, i.e.,  $< 1\%$ . A similar dilemma was encountered in diluted magnetic oxides (DMOs) such as Co-doped ZnO and  $\text{TiO}_2$ , where ferromagnetism has been observed in thin films but not in bulk materials. The origin of ferromagnetism<sup>7</sup> in these DMO systems is yet to be established.

The search for bulk DMS or DMO materials and the investigation of their physical properties may shed light on the origin of ferromagnetism in their thin-film counterparts. Furthermore, the availability of bulk specimens would enable the use of conventional magnetic probes such as nuclear magnetic resonance (NMR) and neutron scattering, to provide complementary information at a microscopic level. The synthesis of bulk DMS or DMO specimens therefore becomes necessary. Accordingly, Deng *et al.*<sup>9</sup> followed a theoretical proposal by Masek *et al.*<sup>10</sup> and doped Mn into the direct-gap semiconductor  $\text{LiZnAs}$ , thereby successfully synthesizing a bulk I-II-V DMS system,  $\text{Li}(\text{Zn,Mn})\text{As}$ , with ferromagnetic  $T_C$

up to 50 K,<sup>9</sup> and a cubic crystal structure not identical but very similar to that of the 111-type  $\text{LiFeAs}$  (Ref. 11) and  $\text{NaFeAs}$  (Ref. 12) superconductors.  $\text{Li}(\text{Zn,Mn})\text{As}$  exhibits a very small coercive field of 50 Oe, similar to that of (Ga,Mn)As.

Additionally, Deng *et al.*<sup>9</sup> demonstrated that hole carriers mediate ferromagnetism in both  $\text{Li}(\text{Zn,Mn})\text{As}$  and (Ga,Mn)As with exchange interactions of comparable magnitude. The growth of  $\text{Li}(\text{Zn,Mn})\text{As}$  compounds, however, suffers from difficulties in the precise control of Li concentrations, making it difficult to understand the interplay between charge carriers and spins.<sup>9</sup> Recently, Zhao *et al.*<sup>13</sup> reported another ferromagnetic DMS system,  $(\text{Ba,K})(\text{Zn,Mn})_2\text{As}_2$ , with  $T_C$  up to  $\sim 200$  K and a crystal structure identical to that of the 122-type  $(\text{Ba,K})\text{Fe}_2\text{As}_2$  superconductors.<sup>14</sup> In this Rapid Communication, we report the successful fabrication of a different bulk DMS material,  $(\text{La}_{1-x}\text{Ba}_x)(\text{Zn}_{1-x}\text{Mn}_x)\text{AsO}$ , with  $T_C$  up to 40 K and a crystal structure identical to that of the 1111-type FeAs superconductor  $\text{LaFeAsO}$ .<sup>15</sup> This constitutes the third example of a bulk DMS system structurally related to a family of FeAs superconductors.

Chemically stable Ba and Mn atoms are doped into the parent direct-gap ( $\sim 1.5$  eV) semiconductor  $\text{LaZnAsO}$  (Ref. 16) to introduce charge carriers and spins, respectively. The system remains paramagnetic for Mn concentrations up to 10% in the absence of Ba doping, but with doped charge carriers to mediate magnetic exchange, static ferromagnetic order develops in  $(\text{La}_{1-x}\text{Ba}_x)(\text{Zn}_{1-x}\text{Mn}_x)\text{AsO}$  below  $T_C \sim 40$  K as confirmed microscopically by  $\mu\text{SR}$ . Semiconducting behavior exists for concentrations up to  $x = 0.20$ , and pronounced magnetic hysteresis with a coercive field of  $\sim 1$  T has also been observed. Despite the striking difference between the two-dimensional (2D) character of  $(\text{La}_{1-x}\text{Ba}_x)(\text{Zn}_{1-x}\text{Mn}_x)\text{AsO}$  and the three-dimensional (3D) structure of  $\text{Li}(\text{Zn,Mn})\text{As}$  and

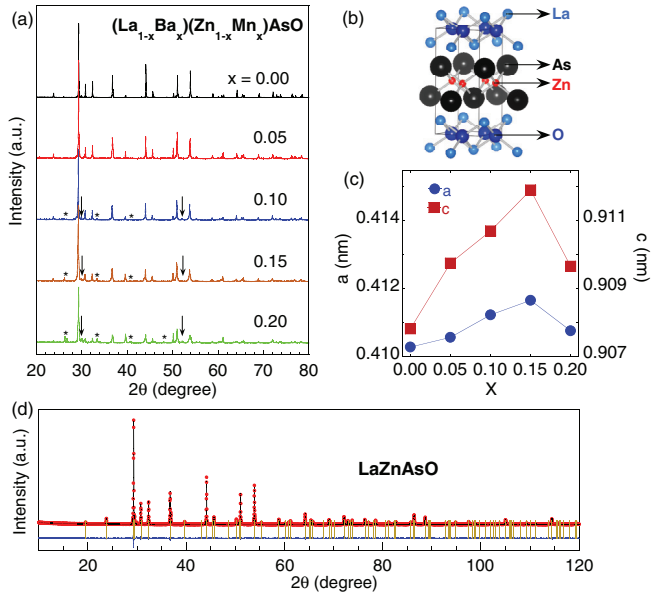


FIG. 1. (Color online) (a) X-ray diffraction pattern of  $(\text{La}_{1-x}\text{Ba}_x)(\text{Zn}_{1-x}\text{Mn}_x)\text{AsO}$ . Traces of impurities  $\text{La}_2\text{O}_3$  ( $\downarrow$ ) and  $\text{ZnAs}_2$  ( $*$ ) are marked for  $x \geq 0.1$ . (b) Crystal structure of  $\text{LaZnAsO}$  ( $P4/nmm$ ). (c) Lattice constants for the  $a$  axis (blue filled circles) and  $c$  axis (red filled squares) of  $(\text{La}_{1-x}\text{Ba}_x)(\text{Zn}_{1-x}\text{Mn}_x)\text{AsO}$ . (d) X-ray diffraction pattern of  $\text{LaZnAsO}$  with Rietveld analyses.

(Ga,Mn)As, all three systems exhibit exchange interactions and ordered moments of similar magnitude.

Polycrystalline specimens of  $(\text{La}_{1-x}\text{Ba}_x)(\text{Zn}_{1-x}\text{Mn}_x)\text{AsO}$  were synthesized through the solid-state reaction method. High-purity samples of La, Zn, and As were mixed and heated to  $900^\circ\text{C}$  in an evacuated silica tube to produce the intermediate products  $\text{LaAs}$  and  $\text{ZnAs}$ , which were mixed with  $\text{ZnO}$ ,  $\text{BaO}_2$ , and Mn with nominal concentrations and slowly heated up to  $1150^\circ\text{C}$ , where the mixture was held for 40 h before cooling at  $10^\circ\text{C/h}$  to room temperature. The polycrystals were characterized via x-ray diffraction and dc magnetization with a Quantum Design superconducting quantum interference device (SQUID). The electrical resistance was measured on sintered pellets with the typical four-probe method.  $\mu\text{SR}$  measurements were performed at the Paul Scherrer Institute and TRIUMF.

The crystal structure and x-ray diffraction patterns are shown in Fig. 1. Bragg peaks from the parent compound  $\text{LaZnAsO}$  can be well indexed by a  $\text{ZrCuSiAs}$ -type tetragonal crystal structure (space group  $P4/nmm$ ), indicating that  $\text{LaZnAsO}$  is isostructural to  $\text{LaFeAsO}$ , the parent compound of the 1111-type family of Fe-based high-temperature superconductors.<sup>15</sup> The Zn atoms, each one tetrahedrally coordinated to four As atoms, form parallel square lattices in the  $ab$  plane, separated along the  $c$  axis by  $\text{LaO}$  layers, resulting in the compound's quasi-2D nature. The lattice parameters were found to be  $a = 4.1027 \text{ \AA}$  and  $c = 9.0781 \text{ \AA}$ , consistent with the previously reported values  $a = 4.10492 \text{ \AA}$  and  $c = 9.08178 \text{ \AA}$ ,<sup>17</sup> and within 5% of the  $\text{LaFeAsO}$  lattice parameters  $a = 4.0355 \text{ \AA}$  and  $c = 8.7393 \text{ \AA}$ .<sup>15</sup> The lattice parameters monotonically increase with Ba and Mn doping up to  $x = 0.15$ , indicating the successful solid solution of (La,Ba) and (Zn,Mn). Impurity

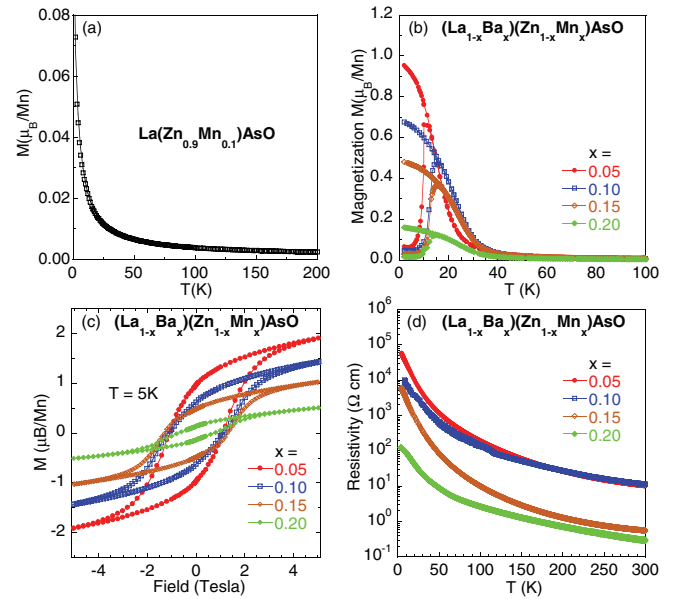


FIG. 2. (Color online) (a) The magnetization  $M$  for  $\text{LaZn}_{0.9}\text{Mn}_{0.1}\text{AsO}$ , without charge doping; the solid line represents the Curie-Weiss law. (b)–(d) Results on  $(\text{La}_{1-x}\text{Ba}_x)(\text{Zn}_{1-x}\text{Mn}_x)\text{AsO}$ : (b)  $M$  obtained in zero-field cooling (ZFC) and field cooling (FC) in an external field of 1000 Oe. (c) The isothermal magnetization measured at 5 K. (d) The electrical resistivity.

phases of  $\text{La}_2\text{O}_3$  and  $\text{ZnAs}_2$  start to appear at  $x = 0.1$  and grow prominently through  $x = 0.20$ , as marked by the arrows and stars in Fig. 1(a).

In Fig. 2(b), we show the zero-field-cooled (ZFC) and field-cooled (FC) measurements of the dc magnetization  $M$  for  $B_{\text{ext}} = 1000 \text{ Oe}$ . A significant increase in  $M$  is observed at temperatures of 30–40 K, and the ZFC and FC curves split at low temperatures for all doping levels. Interestingly, we do not observe such features in Mn-doped  $\text{LaZnAsO}$ ,  $\text{LaZn}_{0.9}\text{Mn}_{0.1}\text{AsO}$ , as shown by the magnetization curve in Fig. 2(a). Instead,  $\text{LaZn}_{0.9}\text{Mn}_{0.1}\text{AsO}$  remains paramagnetic down to 2 K, where  $M$  is about an order of magnitude smaller than for  $(\text{La}_{0.9}\text{Ba}_{0.1})(\text{Zn}_{0.9}\text{Mn}_{0.1})\text{AsO}$ . This indicates that although doping with Mn introduces local moments, the ferromagnetic ordering will not develop unless the spins are mediated by carriers arising from (La,Ba) substitutions. This picture is similar to the case of the (Ga,Mn)As system where Zener's model<sup>18</sup> is proposed as one candidate to explain the ferromagnetism. In this theoretical model, RKKY-like interactions of Mn spins are effectively mediated by hole carriers in the valence band.

The saturation moment has a maximum of  $0.95\mu_B/\text{Mn}$  for  $x = 0.05$  and decreases monotonically with increasing  $x$ , falling to a value of  $0.17\mu_B/\text{Mn}$  for  $x = 0.20$ . This likely results from competition between the RKKY interaction, whose first oscillation period supports ferromagnetic coupling, and nearest-neighbor (NN) antiferromagnetic coupling via direct exchange interaction. For  $x = 0.1$ , the probability of finding two Mn atoms at NN Zn sites is  $P(N;x) = C_N^4 x^N (1-x)^N = 29.16\%$ , where  $N = 1$  and  $x = 0.1$ . The direct antiferromagnetic coupling between the Mn-Mn pairs

causes antiferromagnetic ordering in  $\text{LaMnAsO}$  at  $T_N = 317$  K.<sup>19</sup>

We fit the temperature dependence of  $M$  above  $T_C$  to a Curie-Weiss law. The effective paramagnetic moment is about  $(4-5)\mu_B/\text{Mn}$ , as expected for fully magnetic individual  $\text{Mn}^{2+}$  moments. The isothermal magnetization of  $(\text{La}_{1-x}\text{Ba}_x)(\text{Zn}_{1-x}\text{Mn}_x)\text{AsO}$  at 5 K is plotted in Fig. 2(c). The parallelogram-shaped hysteresis loops show coercive fields of 1.06, 1.14, 1.28, and 0.71 T for  $x = 0.05, 0.10, 0.15,$  and  $0.20$ , respectively, much larger than the  $\sim 50$  Oe coercive field in the cubic  $\text{Li}_{1.1}(\text{Zn}_{0.97}\text{Mn}_{0.03})\text{As}$  (Ref. 9) and  $(\text{Ga}_{0.965}\text{Mn}_{0.035})\text{As}$ .<sup>1</sup> The large coercive field is also reflected in the large differences between the ZFC and FC curves at low temperature [Fig. 2(b)]. The 2D crystal structure of  $(\text{La}_{1-x}\text{Ba}_x)(\text{Zn}_{1-x}\text{Mn}_x)\text{AsO}$  may cause the large coercive field, as a similar situation was found in  $(\text{Ba},\text{K})(\text{Zn},\text{Mn})_2\text{As}_2$ , another 2D DMS system.<sup>13</sup> Efforts are currently under way to generate single crystals to further investigate the anisotropic properties within the  $ab$  plane and along the  $c$  axis.

In Fig. 2(d), we show electrical resistivity measurements for  $(\text{La}_{1-x}\text{Ba}_x)(\text{Zn}_{1-x}\text{Mn}_x)\text{AsO}$ . All samples display typical semi-conducting behavior over the entire temperature range. The resistivity decreases as more carriers are introduced through higher charge doping levels. For  $x = 0.05$ , the resistivity is on the order of  $10^4 \Omega \text{ cm}$ , two orders of magnitude larger than that of  $\text{Li}(\text{Zn},\text{Mn})\text{As}$ .<sup>9</sup> This large resistivity precluded Hall effect measurements on these polycrystalline specimens. In recent papers,<sup>20,21</sup> Liu *et al.* observed Kondo-like behavior in Mn-doped  $\text{CaNiGe}$  and  $\text{CaNiGeH}$ , where the resistivity decreases linearly with decreasing temperature down to 20 K and then increases upon further cooling. This is in contrast to the behavior observed in our compounds.

The availability of bulk specimens enabled us to perform conventional  $\mu\text{SR}$  experiments on  $(\text{La}_{1-x}\text{Ba}_x)(\text{Zn}_{1-x}\text{Mn}_x)\text{AsO}$ . To determine the nature of the magnetic order, we conducted zero-field (ZF), longitudinal-field (LF), and weak-transverse-field (WTF)  $\mu\text{SR}$  measurements for  $x = 0.05$  and ZF and WTF measurements for  $x = 0.1$ . Figure 3(a) displays the time spectra of ZF  $\mu\text{SR}$  for  $x = 0.05$ , showing a rapid increase of muon spin relaxation for temperatures below  $T \sim 30$  K. Several interesting differences are observed between the current results and the ZF  $\mu\text{SR}$  time spectra from the cubic  $\text{Li}_{1.1}(\text{Zn}_{0.95}\text{Mn}_{0.05})\text{As}$ , as illustrated in Fig. 3(c) [adapted from Fig. 3(a) of Ref. 9]. The spectra for the 111-type system in Fig. 3(c) are well described by the sum of a static relaxation function representing the magnetically ordered volume and an exponentially decaying dynamic relaxation function representing the remaining volume in the paramagnetic phase. The time spectra of the present 1111-type system exhibit characteristic signatures of dynamic slowing down followed by static magnetic order, behavior also observed in the spin glasses  $\text{AuFe}$  and  $\text{CuMn}$ .<sup>22</sup> Despite the imperfections of the fit, evidenced by the differences between the data and the fit curves in Fig. 3(a), we plot in Figs. 3(b) and 3(d) the refined static random field amplitude  $a_s$  and dynamic relaxation rate  $\lambda_d$  found in the relaxation function given in Eq. (24) of Ref. 22.

To further study the dynamic spin fluctuations, we performed LF  $\mu\text{SR}$  measurements on the 1111-type DMS system

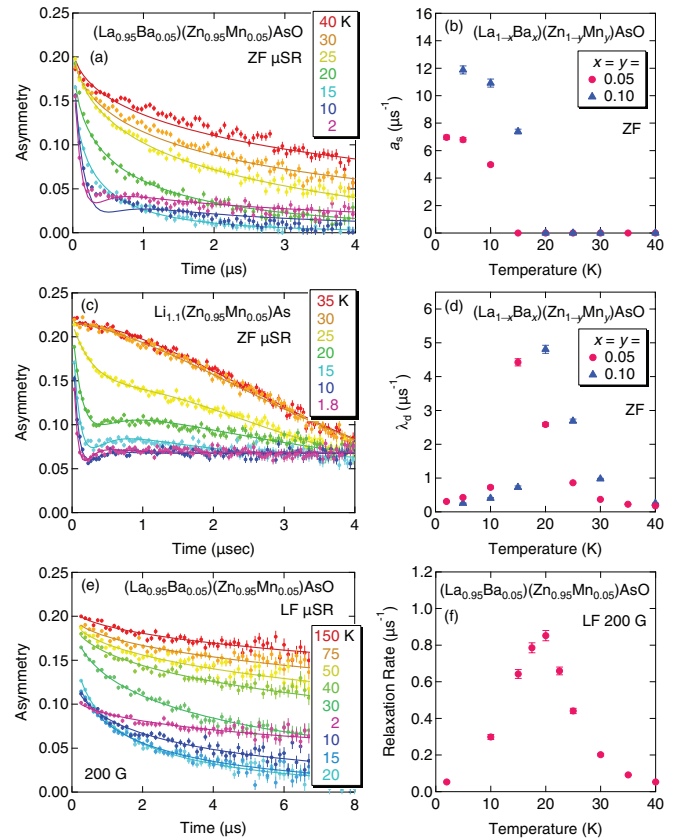


FIG. 3. (Color online) Zero-field  $\mu\text{SR}$  time spectra of (a)  $(\text{La}_{0.95}\text{Ba}_{0.05})(\text{Zn}_{0.95}\text{Mn}_{0.05})\text{AsO}$  (present work) and (c)  $\text{Li}_{1.1}(\text{Zn}_{0.95}\text{Mn}_{0.05})\text{As}$  (adapted from Ref. 9). The solid lines in (a) show a fit to a dynamic-static relaxation function [Eq. (24) of Ref. 22] with the static local field amplitude parameter  $a_s$  shown in (b) and the dynamic relaxation rate parameter  $\lambda_d$  in (d). The solid lines in (c) represent a fit to the “volume fraction model” described in Ref. 9. (b) and (d) also include the results for  $(\text{La}_{0.9}\text{Ba}_{0.1})(\text{Zn}_{0.9}\text{Mn}_{0.1})\text{AsO}$ . (e) shows the time spectra of LF  $\mu\text{SR}$  in  $(\text{La}_{0.95}\text{Ba}_{0.05})(\text{Zn}_{0.95}\text{Mn}_{0.05})\text{AsO}$  with a longitudinal field of 200 G and (f) shows the muon spin relaxation rate  $1/T_1$  due to dynamic spin fluctuations.

with  $x = 0.05$  in a LF of 200 G. Analysis of the time spectra displayed in Fig. 3(e) yields the LF relaxation rate  $1/T_1$  shown in Fig. 3(f), which exhibits a clear peak at  $T \sim 15-20$  K, consistent with the peak temperature of  $\lambda_d$  in ZF [Fig. 3(d)] and the onset temperature of the static spin freezing represented by  $a_s$  [Fig. 3(b)]. ZF  $\mu\text{SR}$  results for  $x = 0.1$  yield similar results for  $a_s$  and  $\lambda_d$ , as shown in Figs. 3(b) and 3(d). LF  $\mu\text{SR}$  measurements were not performed on the  $x = 0.1$  system due to beam-time constraints. We note that for both  $x = 0.05$  and  $x = 0.1$ , the onset temperature of  $a_s$  in ZF and the “spin freezing” temperature indicated by the peaks of  $\lambda_d$  in ZF and  $1/T_1$  in LF agree well with the temperature below which the FC and ZFC magnetizations in Fig. 2(b) show a remarkable departure.

In general, history-dependent behavior can be found both in many regular ferromagnets due to the formation and motion of magnetic domains,<sup>23</sup> and in spin glasses due to multiple minima of the free energy as a function of spin configurations.<sup>24</sup> In some cases the  $z$  component of the spin behaves as a ferromagnet while the  $x$  and  $y$  components behave

as spin glasses.<sup>24,25</sup> The detailed discrimination of these three different cases requires not only the magnetization data but also neutron scattering results for spatial spin correlations. Since a magnetic neutron scattering signal cannot be observed due to the spatially dilute Mn moments and lack of single-crystal specimens, there is no definite evidence at this moment to allow distinguishing between ferromagnetic and spin-glass states for the present system.

Practically speaking, however, there is a clear difference between typical ferromagnets and spin glasses in the magnitudes of their saturation moments in the ground state at low temperatures, obtained in zero field after training in high external magnetic fields. In many ferromagnets, the remanent magnetization value is in the order of  $1\mu_B$  per magnetic atom, while in typical dilute alloy spin glasses, it is  $0.01\mu_B$  per magnetic atom or less.<sup>26–28</sup> In the present system, this remanent magnetization is approximately  $1\mu_B$  per Mn, as shown in Fig. 2(c). Therefore, we tentatively assign the present system as a ferromagnet, rather than as a spin glass.

Use of the so-called spin-glass relaxation function<sup>22</sup> to fit the  $\mu$ SR data does not provide any distinction between ferromagnetic and spin-glass systems, especially for cases with spatially dilute magnetic moments. For example, the earlier  $\mu$ SR results on the well-established ferromagnets (Ga,Mn)As fitted the spin-glass relaxation function quite well.<sup>8</sup>

Analyzed with either the volume fraction fitting used in the 111-type DMSs,<sup>9</sup> the 122-type DMSs,<sup>13</sup> and (Ga,Mn)As systems<sup>8</sup> or the dynamic spin freezing model used in the present 1111-type system, the ZF  $\mu$ SR results indicate that these systems all achieve static magnetic order throughout nearly the entire volume at low temperatures. A closely linear relationship between the local field amplitude parameter  $a_s$  and the Curie temperature  $T_C$  was first noticed in (Ga,Mn)As [Fig. 3(d) of Ref. 8] and Li(Zn,Mn)As [Fig. 3(d) of Ref. 9]. In Fig. 4, we plot  $a_s$  versus  $T_C$  for the two former systems, the 122-type system (Ba,K)(Zn,Mn)<sub>2</sub>As<sub>2</sub>,<sup>13</sup> and the present (La,Ba)(Zn,Mn)AsO system. The universal linear trend suggests that the exchange interaction supporting ferromagnetic coupling in these systems has a common origin and comparable magnitude for a given spatial density of ordered moments.

Magnetization, transport, and  $\mu$ SR studies carried out in (Ga<sub>1-x</sub>Mn<sub>x</sub>)As (Ref. 8) demonstrated that ferromagnetic order is achieved for small Mn concentrations ( $x = 0.012–0.030$ ) even before the system undergoes the semiconductor-to-metal transition. In other words, hole carriers that are not fully delocalized can mediate the ferromagnetic exchange interaction with magnitude comparable to that in the case of full delocalization. It is interesting to note that the quasi-2D 1111-type (present work) and 122-type<sup>13</sup> DMS systems both exhibit ferromagnetism with relatively high  $T_C$  while the charge carriers still remain semiconducting. The average size

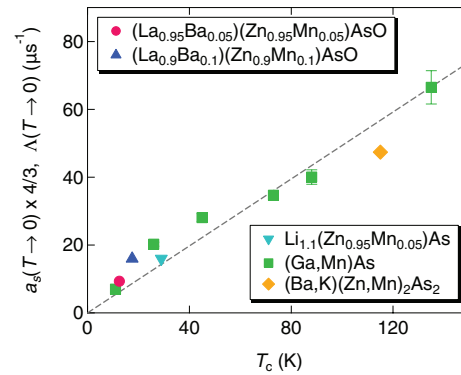


FIG. 4. (Color online) Correlation between the static internal field parameter  $a_s$  determined at  $T = 2$  K by zero-field  $\mu$ SR versus the ferromagnetic Curie temperature  $T_C$  observed in (Ga,Mn)As (Ref. 8), Li(Zn,Mn)As (Ref. 9), (La,Ba)(Zn,Mn)AsO (the present work), and (Ba,K)(Zn,Mn)<sub>2</sub>As<sub>2</sub> (Ref. 13). The nearly linear correlation indicates a common mechanism for the ferromagnetic exchange interaction.

of ordered Mn moments in the 1111-type and 122-type systems is significantly smaller than in (Ga,Mn)As with  $T_C$  above  $\sim 40$  K. This feature suggests that some of the Mn moments are not involved in the percolating ferromagnetic network in the semiconducting DMS systems. The difference between the cubic systems (Ga,Mn)As and Li(Zn,Mn)As and the 2D DMS systems may also indicate that metallic conduction is easier to achieve in 3D systems due to the lower percolation threshold.

In summary, we reported the synthesis of the 1111-type DMS ferromagnet (La<sub>1-x</sub>Ba<sub>x</sub>)(Zn<sub>1-x</sub>Mn<sub>x</sub>)AsO, as the third DMS family which has a direct counterpart among the FeAs superconductor families. As discussed in earlier papers,<sup>9,13</sup> the common crystal structure and excellent lattice matching open doors to the future development of junction devices based on the companion ferromagnetic and superconducting materials. In parallel with the present study, the Han *et al.* have synthesized another “1111” DMS ferromagnet, (La,Ba)(Zn,Mn)SbO, which will be reported separately.<sup>29</sup>

The work at Zhejiang University was supported by the National Basic Research Program of China (Grant No. 2011CBA00103), the NSFC (Grant No.11274268), the Zhejiang Provincial NSFC (Grant No.LY12A04006), and the Fundamental Research Funds for Central Universities (Grant No. 2013QNA3016); at IOP in Beijing by the NSFC and MOST; at Columbia by the U.S. NSF PIRE (Partnership for International Research and Education, Grant No. OISE-0968226) and Grant No. DMR-1105961; the JAEA Reimei Project at IOP, Columbia, PSI, and McMaster; and NSERC and CIFAR at McMaster. We would like to thank C. Cao, A. Fujimori, B. Gu, S.Maekawa, and H. Suzuki for helpful discussions.

\*ningfl@zju.edu.cn

<sup>1</sup>H. Ohno, A. Shen, F. Matsukura, A. Oiwa, A. Endo, S. Katsumoto, and Y. Iye, *Appl. Phys. Lett.* **69**, 363 (1996).

<sup>2</sup>T. Jungwirth, J. Sinova, J. Masek, J. Kucera, and A. H. MacDonald, *Rev. Mod. Phys.* **78**, 809 (2006).

<sup>3</sup>T. Dietl, *Nat. Mater.* **9**, 965 (2010).

<sup>4</sup>I. Zutic, J. Fabian, and S. Das Sarma, *Rev. Mod. Phys.* **76**, 323 (2004).

<sup>5</sup>M. Wang, R. P. Campion, A. W. Rushforth, K. W. Edmonds, C. T. Foxon, and B. L. Gallagher, *Appl. Phys. Lett.* **93**, 132103 (2008).

- <sup>6</sup>N. Samarth, *Nat. Mater.* **9**, 955 (2010).
- <sup>7</sup>S. Chambers, *Nat. Mater.* **9**, 956 (2010).
- <sup>8</sup>S. R. Dunsiger, J. P. Carlo, T. Goko, G. Nieuwenhuys, T. Prokscha, A. Suter, E. Morenzoni, D. Chiba, Y. Nishitani, T. Tanikawa, F. Matsukura, H. Ohno, J. Ohe, S. Maekawa, and Y. J. Uemura, *Nat. Mater.* **9**, 299 (2010).
- <sup>9</sup>Z. Deng *et al.*, *Nat. Commun.* **2**, 422 (2011).
- <sup>10</sup>J. Masek, J. Kudrnovsky, F. Maca, B. L. Gallagher, R. P. Champion, D. H. Gregory, and T. Jungwirth, *Phys. Rev. Lett.* **98**, 067202 (2007).
- <sup>11</sup>X. C. Wang, Q. Q. Liu, Y. Y. Lv, W. B. Gao, S. M. Feng, L. X. Yang, R. C. Yu, F. Y. Li, and C. Q. Jin, *Solid State Commun.* **148**, 538 (2008).
- <sup>12</sup>D. R. Parker, M. J. Pitcher, P. J. Baker, I. Franke, T. Lancaster, S. J. Blundell, and S. J. Clarke, *Chem. Commun. (Cambridge)* **2009**, 2189.
- <sup>13</sup>K. Zhao, Z. Deng, X. C. Wang, W. Han, J. L. Zhu, X. Li, Q. Q. Liu, T. Goko, B. Frandsen, L. Liu, F. L. Ning, Y. J. Uemura, H. Dabkowska, G. M. Luke, H. Luetkens, E. Morenzoni, S. R. Dunsiger, A. Senyshyn, P. Boeni, and C. Q. Jin, *Nat. Commun.* **4**, 1422 (2013).
- <sup>14</sup>D. C. Johnston, *Adv. Phys.* **59**, 803 (2010).
- <sup>15</sup>Y. Kamihara, T. Watanabe, M. Hirano, and H. Hosono, *J. Am. Chem. Soc.* **130**, 3296 (2008).
- <sup>16</sup>K. Kayanuma, R. Kawamura, H. Hiramatsu, H. Yanagi, M. Hirano, T. Kamiya, and H. Hosono, *Thin Solid Films* **516**, 5800 (2008).
- <sup>17</sup>Y. Takano, S. Komaatsuzaki, H. Komasaki, T. Watanabe, Y. Takahashi, and K. Takase, *J. Alloys Compd.* **451**, 467 (2008).
- <sup>18</sup>T. Dietl, H. Ohno, F. Matsukura, J. Cibert, and D. Ferrand, *Science* **287**, 1019 (2000).
- <sup>19</sup>N. Emery, E. J. Wildman, J. M. S. Skakle, A. C. Mclaughlin, R. I. Smith, and A. N. Fitch, *Phys. Rev. B* **83**, 144429 (2011).
- <sup>20</sup>X. F. Liu, S. Matsuishi, S. Fujitsu, and H. Hosono, *Phys. Rev. B* **84**, 214439 (2011).
- <sup>21</sup>X. F. Liu, S. Matsuishi, S. Fujitsu, T. Ishigaki, T. Kamiyama, and H. Hosono, *J. Am. Chem. Soc.* **134**, 11687 (2012).
- <sup>22</sup>Y. J. Uemura, T. Yamazaki, D. R. Harshman, M. Senba, and E. J. Ansaldo, *Phys. Rev. B* **31**, 546 (1985).
- <sup>23</sup>N. W. Ashcroft and N. D. Mermin, *Solid State Physics* (Holt, Rinehart and Winston, New York, 1976).
- <sup>24</sup>K. H. Fischer, and J. A. Hertz, *Spin Glasses* (Cambridge University Press, Cambridge, 1991).
- <sup>25</sup>I. Mirebeau, in *Recent Progress in Random Magnets*, edited by D. H. Ryan (World Scientific, Singapore, 1992), p. 41.
- <sup>26</sup>J. L. Tholence, and R. Tournier, *J. Phys. (Paris)* **35**, C4-229 (1974).
- <sup>27</sup>J. J. Prejean, M. J. Joliclerc, and P. Monod, *J. Phys. (Paris)* **41**, 427 (1980).
- <sup>28</sup>P. Monod, J. J. Prejean, and B. Tissier, *J. Appl. Phys.* **50**, 7324 (1979).
- <sup>29</sup>W. Han, F. L. Ning, Y. J. Uemura, and C. Q. Jin (unpublished).